Influence of the surface band structure on electron emission spectra from metal surfaces

C. D. Archubi,[1] M. N. Faraggi,[1] V. M. Silkin,[2,3,4] and M. S. Gravielle[1]

[1]*Instituto de Astronomía y Física del Espacio (National Scientific and Technical Research Council, Universidad de Buenos Aires), Casilla de Correo 67, Sucursal 28, C1428EGA Buenos Aires, Argentina*

[2]*Donostia International Physics Center, 20018 San Sebastián, Spain*

[3]*Departamento de Física de Materiales, Facultad de Ciencias Químicas, Universidad del País Vasco, Apdo. 1072, 20080 San Sebastián, Spain*

[4]*IKERBASQUE, Basque Foundation for Science, 48011 Bilbao, Spain*

(Received 22 October 2013; revised manuscript received 25 February 2014; published 21 April 2014)

Electron distributions produced by grazing impact of fast protons on Mg(0001), Cu(111), Ag(111), and Au(111) surfaces are investigated, focusing on the effects of the electronic band structure. The process is described within the band-structure-based approximation, which is a perturbative method that includes an accurate representation of the electron-surface interaction, incorporating information of the electronic band structure of the solid. For all the studied surfaces, the presence of partially occupied surface electronic states produces noticeable structures in double-differential—energy- and angle-resolved—electron emission probabilities from the valence band. For Mg, Cu, and Ag these structures remain visible in electron emission spectra after adding contributions coming from core electrons, which might make possible their experimental detection, but for Au they are hidden by inner-shell emission.

DOI: 10.1103/PhysRevB.89.155421 PACS number(s): 34.35.+a, 79.20.Rf

I. INTRODUCTION

When a charged particle moves parallel to a metal surface different processes may take place [1,2], like energy loss of the ion, charge transfer between particle and metal, inner-shell and valence-band electronic excitations, and secondary electron emission. In particular, the interaction of the projectile with valence electrons of the solid produces a rearrangement of the charges inside the material, a dynamic process that gives rise to one-particle electronic transitions (electron-hole excitations) and collective excitation (plasmon) processes. For decades these processes were studied using simple representations of the unperturbed electronic states of the surface, while the emphasis was set on the description of the response of the many-electron system to the external perturbation. However, recent experimental and theoretical works showed that the band structure of different metal surfaces plays an important role in projectile induced processes [3–17]. In surfaces like Cu(111), Ag(111), and Au(111) it was found that the energy lost by charged particles moving at long distances from the surface is dominated by electron-hole excitations involving partially occupied surface states [11]. Also in the case of Mg(0001) the finite width of the surface plasmon modifies the behavior of the energy loss at long distances from the surface, being relevant for the study of the interaction mechanisms between charged particles and the internal walls of microcapilars [13,18].

In most of the above-mentioned articles, the influence of the surface band structure on energy-loss processes was investigated making use of the dielectric formalism. This formalism involves a quantum calculation of the surface response function but describes the stopping of the incident particle by means of classical electromagnetism laws. Here we are interested in studying individual electronic transitions induced by the projectile. In particular, the work focuses on angle- and energy-resolved electron emission distributions produced by grazing impact of swift protons on metal surfaces. Such spectra are expected to provide detailed information on the electronic characteristics of the target surface.

To describe the electron emission process from the valence band we employ the band-structure-based (BSB) approximation [19,20], which is derived within the framework of the binary collisional formalism by including a precise representation of the surface interaction. For every individual electronic excitation, the BSB transition matrix is evaluated making use of the electronic states corresponding to the model potential of Ref. [21], which incorporates effects of the band structure of the metal. This potential has been successfully used in several areas [10–13,19–23], reproducing properly the projected energy gap and the energies of the surface and first image states. Within the BSB method, the dynamic response of the medium to the incident charge is obtained from the unperturbed electronic wave functions by using the linear response theory.

In a previous work [20] the BSB approximation was applied to study electron emission induced by grazing incidence of fast protons on a Be(0001) surface. It was found that the distribution of ejected electrons presents prominent signs of the surface band structure, with pronounced shoulders due to the contribution of partially occupied surface electronic states (SESs). In this paper the research is extended to consider electron emission from Cu(111), Ag(111), Au(111), and Mg(0001) surfaces, for which it is foreseeable that band structure effects leave footprints on the electron emission spectra like the ones observed in stopping processes. Contributions from the inner shells of surface atoms, calculated with the continuum-distorted-wave Eikonal-initial-state (CDW-EIS) approximation, are also included in the spectra in order to determine the energy and angular range where band structure effects might be experimentally detected. In addition, with the aim of investigating the dependence on the incidence conditions, the influence of the projectile trajectory is analyzed.

The paper is organized as follows. In Sec. II we summarize the theoretical model, results are presented and discussed in

Sec. III, and Sec. IV contains our conclusions. Atomic units are used unless otherwise stated.

II. THEORETICAL METHOD

We consider a projectile P that impinges grazingly on a metal surface, inducing the one-electron transition $i \to f$, where the state i belongs to the valence band while the state f lays in the continuum. Within the binary collisional formalism, the corresponding transition probability per unit path reads [24]

$$P_{if}(Z) = \frac{2\pi}{v_s}\delta(\Delta)|T_{if}|^2, \tag{1}$$

where Z is the projectile distance to the surface, v_s is the component of the projectile velocity parallel to the surface plane, and the Dirac delta function $\delta(\Delta)$expresses the energy conservation, with

$$\Delta = \vec{v}_s \cdot (\vec{k}_{fs} - \vec{k}_{is}) - (E_f - E_i), \tag{2}$$

$\vec{k}_{is}$ ($\vec{k}_{fs}$) being the initial (final) electron momentum parallel to the surface and E_i (E_f) being the initial (final) electron energy. In Eq. (1) T_{if} represents the T-matrix element, which is evaluated within a first-order perturbation theory as

$$T_{if} = \langle \Phi_f | V | \Phi_i \rangle, \tag{3}$$

where $\Phi_i(\Phi_f)$is the initial (final) unperturbed electronic state, evaluated with the BSB model, and V denotes the perturbative potential produced by the external charge.

By assuming translational invariance in the plane parallel to the surface, the BSB unperturbed states, $\Phi_i = \Phi_{\vec{k}_{is},n_i}$ and $\Phi_f = \Phi_{\vec{k}_{fs},n_f}$, are characterized by the energy with a paraboliclike dispersion $E_{\vec{k}_{s,n}} = k_s^2/2 + \varepsilon_n$ and the wave function

$$\Phi_{\vec{k}_s,n}(\vec{r}) = \frac{1}{2\pi}\exp(i\vec{k}_s.\vec{r}_s)\phi_n(z), \tag{4}$$

where $\vec{r} = (\vec{r}_s, z)$ is the position vector of the active electron, with $\vec{r}_s$ and z being the components of $\vec{r}$ parallel and perpendicular, respectively, to the surface plane. The function $\phi_n(z)$ represents the eigenfunction of the one-dimensional (1D) Schrödinger equation associated with the surface potential of Ref. [21] with eigenenergy ε_n.

By using slab geometry, the eigenfunctions $\phi_n(z)$ can be classified as symmetric (S) or antisymmetric (A) according to the reflection symmetry properties with respect to the center of the slab. They read

$$\phi_n^{(S)}(z) = \frac{1}{\sqrt{L}}c_n^{(S)}(0) + \frac{1}{\sqrt{L}}\sum_{l=1}^{N} c_n^{(S)}(l)\cos\left(\frac{2\pi l}{L}\widetilde{z}\right), \tag{5}$$

$$\phi_n^{(A)}(z) = \frac{1}{\sqrt{L}}\sum_{l=1}^{N} c_n^{(A)}(l)\sin\left(\frac{2\pi l}{L}\widetilde{z}\right), \tag{6}$$

where L is the length of the unit cell, $2N+1$ is the number of basis functions, and the coefficients $c_n^{(j)}(l)$, $j = S, A$, are obtained numerically [11]. The coordinate $\widetilde{z} = z + d_s$ represents the normal distance measured with respect to the center of the slab, which is placed at a distance d_s from the surface plane.

In Eq. (3) the potential V is expressed as $V = V_{Pe} + V_{\rm ind}$, where $V_{Pe} = -Z_P/r_P$ denotes the Coulomb projectile potential, with Z_P being the projectile charge and r_P being the electron-projectile distance, and $V_{\rm ind}$ represents the surface potential induced by the incident ion moving at a distance Z from the surface plane. The potential $V_{\rm ind}$ is obtained from the two-dimensional Fourier transform of the density-density response function, which is calculated within the linear response theory by employing the BSB unperturbed electronic states given by Eq. (4) [11,25].

The differential electron transition probability from the valence band to a given final state f with momentum $\vec{k}_f$, $dP_{vb}/d\vec{k}_f$, is derived by integrating Eq. (1) along the classical projectile path, after adding the contributions coming from the different initial states. That is,

$$\frac{dP_{vb}}{d\vec{k}_f} = \int_{-\infty}^{+\infty} dX \left[\sum_i \rho_e\, \Theta(-E_W - E_i) P_{if}[Z(X)]\right], \tag{7}$$

where $Z(X)$ is the projectile trajectory, with X being the coordinate along the incidence direction; $\rho_e = 2$ takes into account the spin states; and the unitary Heaviside function Θ restricts the initial states to those contained inside the Fermi sphere, with E_W being the work function. Notice that the Dirac delta function of Eq. (1) restricts the allowed initial momenta, making it so that only two different values of k_{is} contribute to every transition $i \to f$ [see Eq. (12) of Ref. [19]]. Additionally, within the BSB model the final electronic states Φ_f present a well-defined momentum only in the direction parallel to the surface plane. Then, in order to determine $\vec{k}_f = (\vec{k}_{fs}, k_{fz})$ it is necessary to define an *effective* electron momentum perpendicular to the surface as $k_{fz} = \sqrt{2\varepsilon_{n_f}}$, where ε_{n_f} is the eigenenergy associated with the final wave function $\phi_{n_f}(z)$. More details of the BSB approximation can be found in Ref. [19].

III. RESULTS

We apply the BSB approximation to investigate electron emission spectra produced by grazing scattering of protons from different metal surfaces—Mg(0001), Cu(111), Ag(111), and Au(111)—considering incidence velocities in the high-energy range, i.e., ranging from 1.5 to 3.5 a.u. At these impact energies, electron capture processes are negligible and protons can be treated as bare ions along the whole path [26]. To evaluate the classical projectile trajectory we employed the Ziegler-Biersack-Littmark potential [27] plus the BSB induced potential, which was derived in a consistent way by using the linear response theory [11].

The differential probability of electron emission from the valence band, $dP_{vb}/d\vec{k}_f$, was obtained from Eq. (7) by interpolating the P_{if} function, given by Eq. (1), from data corresponding to 24 different Z distances. The T_{if} elements were calculated by using the BSB wave functions of Eq. (4), where the wave functions ϕ_n were derived by following the same procedure as in Refs. [19,20,22]. Slabs formed by 40 atomic layers were used for the different targets, while the number of layers associated with the vacuum was chosen as 20 for Cu, Ag, and Au and 10 for Mg. The length of the

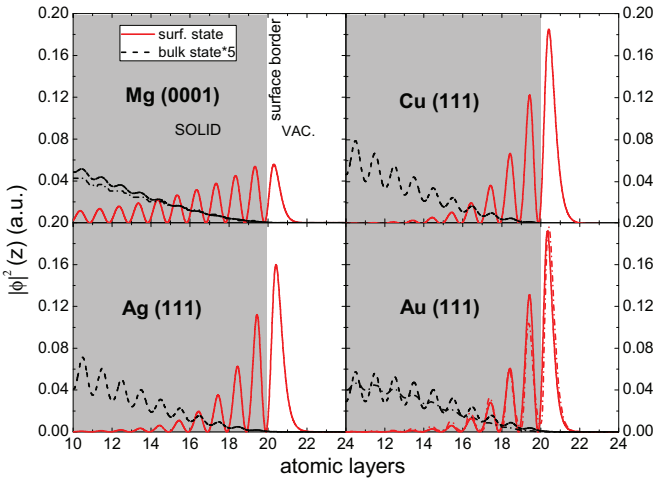

FIG. 1. (Color online) Comparison between the electronic density of the SES and the one corresponding to a bulklike state (multiplied by a factor 5, except in the case of Au) with the lowest-energy value corresponding to $n = 1$ for (a) Mg(0001), (b) Cu(111), (c) Ag(111), and (d) Au(111). Dash-dotted line represents bulk and surface-state DFT results which are added in (a) and (b) as a reference.

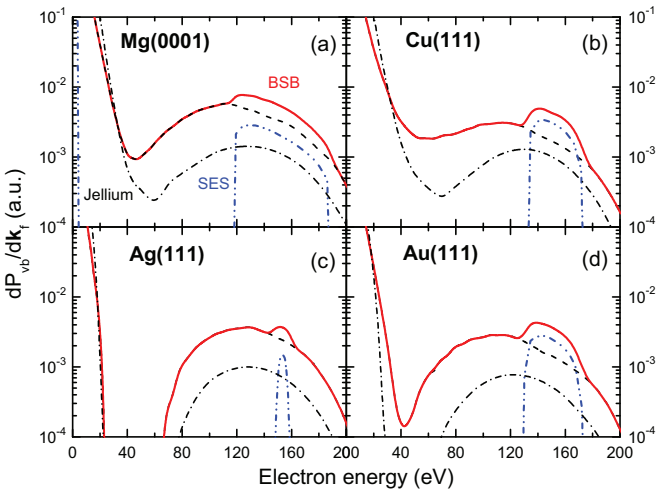

FIG. 2. (Color online) Differential probability of electron emission from the valence band, as a function of the electron energy, for 100-keV protons impinging with the glancing angle $\alpha = 0.1^\circ$ on (a) Mg(0001), (b) Cu(111), (c) Ag(111), and (d) Au(111). The electron ejection angle is $\theta_e = 30^\circ$, measured with respect to the surface in the scattering plane. Solid red line, BSB results including the SES contribution; dashed black line, BSB results without the SES contribution; dash-dot-dotted blue line, SES contribution; dash-dotted black line, results obtained within the jellium model [24].

unit cell (L) considered for every material varies between 250 and 300 a.u. and the sums in Eqs. (5) and (6) run up to $N = 150$ for Cu, Ag, and Au and $N = 140$ for Mg. The effective masses m_n for all the energy bands were set to unity. The Fermi energy level was determined from the work function values reported in Ref. [21]. Notice that all the studied surfaces present SESs that are partially occupied with energy $\varepsilon_{\rm SES}$ according to the Fermi level of -1.50, -0.44, -0.067, and -0.475 eV for Mg(0001), Cu(111), Ag(111), and Au(111), respectively [28,29]. The corresponding charge density distributions, $|\phi_n(z)|^2$, are displayed in Fig. 1. In the same figure we also plot, as an example, the charge density for a bulklike valence state with the lowest energy corresponding to $n = 1$. We have multiplied the bulk results by a factor 5 for the sake of clarity, except for the case of Au. In the case of Mg(0001) and Au(111), curves corresponding to the in-plane averaged charge density distributions derived from *ab initio* density-functional-theory local-density-approximation (DFT-LDA) calculations [14,30,31] are included in the figure. Comparison of these two sets of data shows that the wave functions derived with the model potential are in fairly good agreement with those obtained with the use of a much more elaborated DFT approach. At the same time we would expect that the Mg(0001) SES wave-function decay rate is better reproduced by the model potential [21]. This is explained by a well-known energy-gap-description problem of the DFT-LDA approach, which produces an energy gap in Mg(0001) two times smaller than measured in the photoemission experiment [28]. Hence, the reflectivity of the crystal is significantly underestimated in the DFT-LDA calculation, resulting in the too low decay rate of the SES wave function. Also in Fig. 1 one can note a larger amplitude of the short-wavelength oscillations in bulklike states produced by the lattice potential, which is stronger in the 1D approach. However, we do not expect that this fact strongly affects our results. Regarding the states above the vacuum level, in our model the wave functions of these states are more realistic than simple plane waves frequently assumed for such states. At the same time it was demonstrated [32,33] that in this energy region the electronic structure may deviate substantially from a free-electron-like picture with the corresponding alteration of the wave functions. However, this effect cannot be accounted for in a simplified 1D approach and its description requires a full three-dimensional treatment.

Within the BSB model two $\phi_{n_f}(z)$ functions—the symmetric one and the antisymmetric one—are associated with the same energy ε_{n_f} in the thick slab limit. This representation does not allow us to distinguish electrons emitted inside the solid from those ejected toward the vacuum semispace. Then, as a first estimate we considered that ionized electrons emitted to the vacuum region represent approximately 50% of the total ionized electrons from the valence band [19,22].

With the aim of presenting an overall scenario of the influence of the electronic band structure for the different materials, in Fig. 2 we show $dP_{vb}/d\vec{k}_f$, as a function of the electron energy, for protons impinging on Mg, Cu, Ag, and Au surfaces with the incidence velocity $v = 2$ a.u. and the glancing angle $\alpha = 0.1^\circ$. In the figure, results for the ejection angle $\theta_e = 30^\circ$, measured with respect to the surface in the scattering plane, are displayed by using the same scale for all the cases. These spectra show the typical double-peaked structure associated with soft and binary single-particle collisions, respectively, with conduction electrons [34]. However, in addition to such structures, the BSB curves exhibit a noticeable superimposed bulge in the high-electron-energy region, which disappears completely when partially occupied SESs are not included in

the calculations. The shape and size of this elevation depend on the material, looking like a large shoulder for Mg, Cu, and Au, while for Ag the structure resembles a small protuberance of the electron distribution. We found that the contribution coming from SESs, also shown in the figure, is responsible for the superimposed structure of the electron spectrum. This is due to the fact that SESs present highly peaked electron densities near the surface, as shown in Fig. 1, which favors the electron emission when the projectile moves far from the surface plane. As a result, the SES contribution is more relevant when, in the selvage region, differences between the electronic density associated with the SES and those corresponding to other occupied electronic states are larger, as it happens for the copper, silver, and gold surfaces, for which the differences rise up to a factor larger than 70. On the other hand, when the electron-surface interaction is represented by a finite step potential (the *jellium* model) [24], without taking into account the electronic band structure, the electron emission distributions display a smooth behavior as a function of the electron energy, also observed for Be(0001) surfaces [20].

In order to analyze the angular dependence of the SES contribution, differential probabilities for electron emission from the valence band of Cu(111) are plotted in Fig. 3, as a function of the electron energy, for emission angles θ_e ranging from 20 to 70°. For the smaller θ_e values the SES bulge is placed around the energy of the binary maximum and, when the ejection angle increases, the SES structure moves gradually to the low-energy region. Simultaneously, an additional SES peak arises at low energies, which ends up joined to the SES shoulder for $\theta_e \gtrsim 60°$. This behavior is ruled by the energy conservation imposed by the delta function of Eq. (2), which determines the maximum ($k_{\rm SES}^{(+)}$) and minimum ($k_{\rm SES}^{(-)}$) final momenta reached by transitions from occupied SESs. These momenta verify

$$k_{\rm SES}^{(\pm)} = v_s \cos\theta_e + \sqrt{R_\pm^2 - v_s^2 \sin^2\theta_e}, \qquad (8)$$

where $R_\pm^2 = (k_{\rm SES} \pm v_s)^2 + 2\varepsilon_{\rm SES}$, with $k_{\rm SES} = \sqrt{-2(E_W + \varepsilon_{\rm SES})}$ and with the condition that the value $k_{\rm SES}^{(-)}$ becomes zero when $\sin^2\theta_e > R_{\rm min}^2/v_s^2$. The right-hand side of Eq. (8) decreases when θ_e increases and, consequently, the maximum and minimum energies associated with SES emission shift to lower values.

Even though for all the considered surfaces SES structures are clearly visible in electron emission spectra from the valence band, in experimental electron distributions [35] there is another source of ejected electrons—the inner shells of surface atoms—which might hide SES effects. To evaluate the inner-shell emission yield we employ a semiclassical formalism [34] that describes the multiple collisions of the incident ion with the surface atoms as single encounters with outermost atoms along the projectile path. In the model the core emission probability per unit path is expressed in terms of atomic probabilities, which are evaluated within the CDW-EIS approximation. The CDW-EIS approach is a distorted wave method that accounts for the proper asymptotic conditions [36], including the distortion produced by the projectile in both the initial and final states. The Coulomb projectile potential was shielded with a dynamic screening as

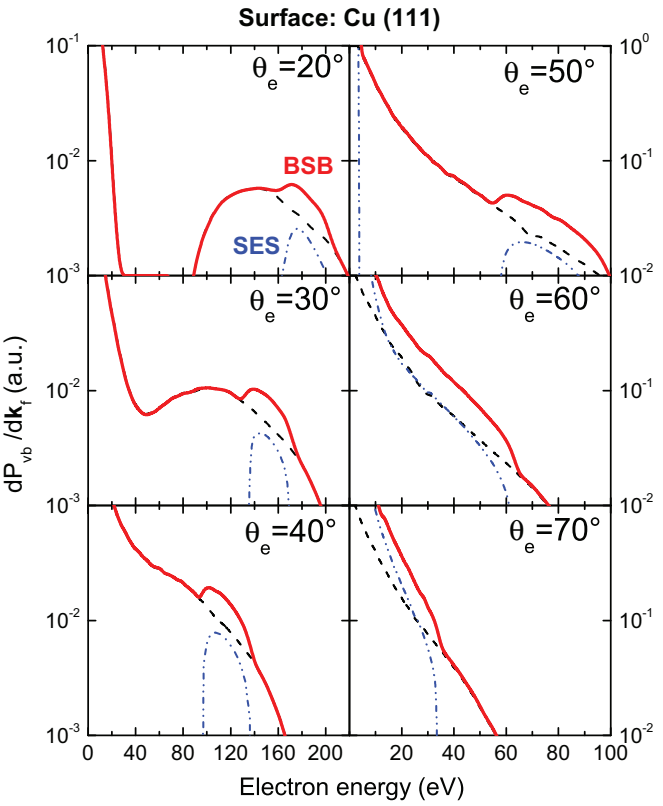

FIG. 3. (Color online) Influence of the SES in differential electron emission probabilities for 100-keV protons impinging on a Cu(111) surface with an incidence angle $\alpha = 0.5°$. Vertical scales of the right (left) panels are indicated on the right (left) side. The electron ejection angles are $\theta_e = 20$, 30, 40, 50, 60, and 70°, respectively, all of them measured with respect to the surface in the scattering plane. Solid red line, BSB electron emission spectrum; dashed black line, BSB electron emission spectrum without including the SES contribution; dash-dot-dotted blue line, SES contribution.

reported in Ref. [37], which was introduced in the calculation by means of a momentum-dependent projectile charge [38]. In the evaluation of the atomic probability we have taken into consideration the full dependence of the CDW-EIS transition amplitude on the impact parameter, that is, not only on the modulus of the impact parameter but also on its direction.

Total emission probabilities obtained as the sum of valence and core contributions are plotted in Fig. 4, together with the partial valence and inner-shell distributions, for electron emission from a Cu(111) surface with different ejection angles. The core emission probability from the copper surface was evaluated by including the 3*d* level only, since contributions coming from deeper shells are expected to be negligible. To represent the 3*d* initial state of Cu we used the Hartree-Fock wave function corresponding to the Cu^+ ion [39], considering that the outermost electron was assigned to the valence band. The final continuum state, associated with the electron ejected from the 3*d* level, was described as a Coulomb wave function with an effective charge satisfying the initial binding energy. The figure shows that core electrons give rise to a probability that decreases evenly when the electron energy

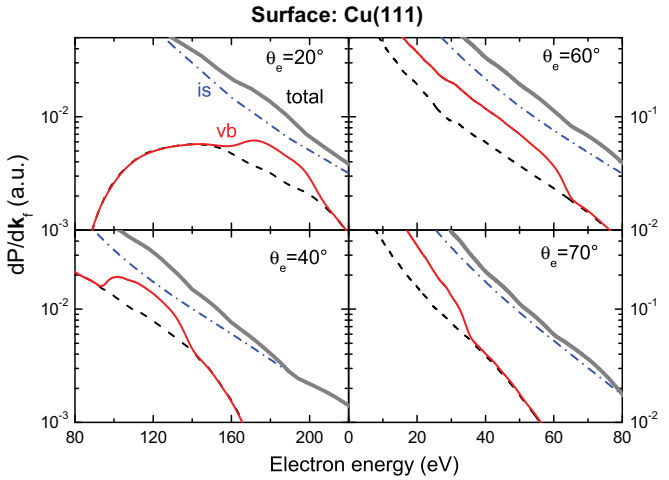

FIG. 4. (Color online) Similar to Fig. 3 for total emission probability, including valence-band and inner-shell contributions. Vertical scales of the right (left) panels are indicated on the right (left) side. The ejection angles are $\theta_e = 20$, 40, 60, and 70°, respectively. Solid thick gray line, total emission probability obtained by adding valence-band and core contributions, as explained in the text; solid thin red line, BSB valence emission probability; dashed black line, BSB probability without including the SES contribution; dot-dashed blue line, inner-shell emission probability.

increases. It represents the main contribution to the electron emission spectra in almost the whole energy and angular range. However, signatures of the SES emission are still present in total electron distributions. At intermediate ejection angles, the SES structure of the valence-band distribution is visible, albeit weakened, in the total emission spectrum, producing an increase of total probability around the SES position that varies between 10 and 25% approximately. In turn, for $\theta_e \gtrsim 60°$ SES effects are reflected as a change in the slope of the electron energy distribution. Notice that under the condition of grazing incidence transport effects are expected to play a minor role [40], at least for the electron ejection angles considered here, and consequently present theoretical spectra might be directly compared with experimental data.

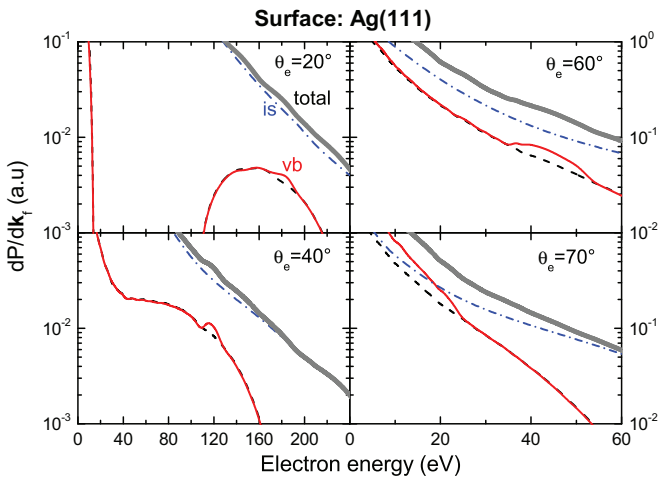

FIG. 5. (Color online) Similar to Fig. 4 for a Ag(111) surface.

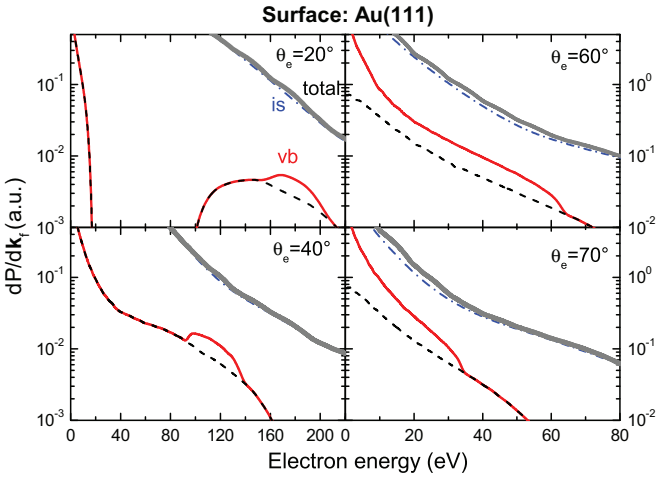

FIG. 6. (Color online) Similar to Fig. 4 for a Au(111) surface.

When the atomic number of surface atoms increases, the inner-shell contribution to the electron emission process augments, as it happens for Ag and Au surfaces, displayed in Figs. 5 and 6, respectively. For silver, inner-shell emission corresponding to the 4*d* level was calculated by using the Hartree-Fock wave function of Ag^+ [39], while for gold the core contribution from the 5*d* level was evaluated by employing the relativistic wave function of Ref. [41]. In both cases, at the smaller ejection angles, core emission represents the dominant mechanism that partially conceals surface band structure effects in electron emission spectra. For Ag(111), a small SES structure is barely perceivable in total electron distributions for ejection angles lower than 60°, while for larger angles the SES contribution produces a change of the slope at low electron energies, also observed for Cu surfaces. However, for Au(111), despite the remarkable contribution of the electron emission from partially occupied SESs, its effects are almost completely covered by the inner-shell contribution.

In contrast, for Mg(0001) valence-band electrons provide the main contribution to the electron emission process, as shown in Fig. 7. In this case, inner-shell emission from

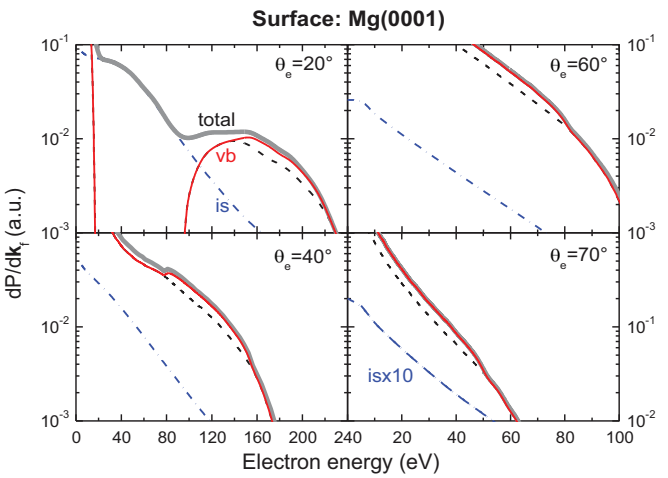

FIG. 7. (Color online) Similar to Fig. 4 for a Mg(0001) surface.

the L shell of Mg cores [42] is more than one order of magnitude lower than the valence-band contribution, except for the lower θ_e values, precisely in the energy region where electron emission from the valence band is forbidden as a result of energy conservation [Eq. (2)]. In such an energy region the inner-shell spectrum for $\theta_e = 20^\circ$ displays still the footprints of the convoy-electron peak [43], which is associated with electrons that move away from the surface in close spatial correlation with the projectile [44,45]. The signatures of the convoy-electron peak disappear when the ejection angle augments, as observed for $\theta_e = 40^\circ$. Then, although SES effects for Mg(0001) are weaker than for the previous surfaces, they are appreciable in total electron distributions for a wide range of ejection angles.

Finally, we address the study of the influence of the incidence conditions on SES effects, taking as a prototype the Cu(111) surface. In Fig. 8(a) we plot $dP_{vb}/d\vec{k}_f$ for protons impinging grazingly on Cu(111) with velocities ranging from $v = 1.5$ to 3.5 a.u. The ejection angle was chosen as $\theta_e = 60^\circ$. We found that the SES shoulder shifts to higher electron energies as the projectile velocity increases, in accord with Eq. (8), but its relative contribution changes moderately as the velocity varies. In Fig. 8(b) we plot $dP_{vb}/d\vec{k}_f$ for the ejection angle $\theta_e = 30^\circ$ considering the projectile velocity $v = 2$ a.u. and different impact angles. For these incidence conditions the distances of minimum approach of the projectile to the surface (topmost atomic layer) are $Z_m = 1.0$, 1.6, 2.9, and 5.0 a.u., respectively, where the longest distance corresponds to smallest incidence angle. Such turn-off positions happen at distances from the surface where the SES density has a significant contribution to the total charge density, explaining the notable effect of this state into the electron transition probability. When projectiles move far away from the surface plane, as it happens for the lower α values, only SES electrons are strongly affected by the external perturbation, giving rise to a remarkable SES contribution. However, when the incidence angle α augments, keeping the velocity as a constant, the SES structure becomes smaller, producing only a smooth shoulder in the electron emission probability for $\alpha = 0.75^\circ$. This behavior is due to the fact that large incidence angles allow protons to reach distances closer to the surface, inducing a strong electron emission also from different occupied electronic states. Similar behavior was also observed for the other surfaces. Then, for the studied surfaces SESs might be experimentally probed by proton impact with glancing angles.

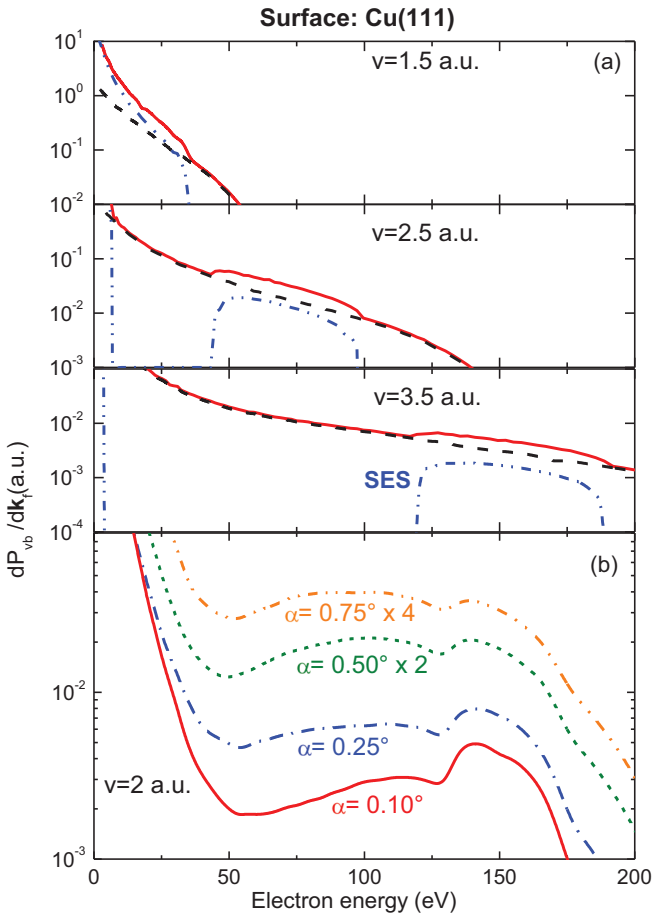

FIG. 8. (Color online) Influence of the incidence conditions on differential electron emission probabilities from the valence band of Cu(111). (a) Different impact velocities, keeping the incidence angle, $\alpha = 0.5^\circ$, as a constant, for the ejection angle $\theta_e = 60^\circ$. (b) Different incidence angles, keeping the impact velocity, $v = 2$ a.u., as a constant, for the ejection angle $\theta_e = 30^\circ$.

IV. CONCLUSIONS

Electron emission spectra produced by grazing incidence of protons on Mg(0001), Ag(111), Cu(111), and Au(111) surfaces have been studied, including valence-band and inner-shell contributions. For all the considered surfaces, BSB differential emission probabilities from the valence band display noticeable structures due to the presence of partially occupied SESs. Such structures are related to the high localization of the electronic density of the SES around the selvage region, which promotes the electron emission process for projectiles moving outside the solid. Consequently, SES structures are more pronounced for glancing incidence angles, moving to higher energies as the incidence velocity increases.

We found that SES structures are clearly visible in total emission spectra for Mg, Cu, and Ag surfaces. However, for Au, band structure effects become softened and even completely covered by the inner-shell emission. We hope the present work will prompt experimental research on the subject.

ACKNOWLEDGMENTS

This work was partially supported by the Consejo Nacional de Investigaciones Científicas y Técnicas; the Agencia Nacional de Promoción Científica y Tecnológica; and the Universidad Nacional de Buenos Aires, Argentina. V.M.S. acknowledges partial support from the University of the Basque Country (Grant No. IT-366-07), the Departamento de Educación del Gobierno Vasco, and the Spanish Ministerio de Ciencia e Innovación (Grant No. FIS2010-19609-C02-01).

[1] A. Arnau *et al.*, Surf. Sci. Rep. **27**, 117 (1997).
[2] H. Winter, Phys. Rep. **367**, 387 (2002).
[3] D. Goebl, D. Valdes, E. Abad, R. C. Monreal, D. Primetzhofer, and P. Bauer, Phys. Rev. B **84**, 165428 (2011).
[4] A. Sindona *et al.*, Surf. Sci. **601**, 1205 (2007).
[5] M. Pisarra, P. Ricardi, A. Cupolillo, A. Sindona, and L. S. Caputi, Nanosci. Nanotechnology Lett. **4**, 1100 (2012).
[6] A. Sindona *et al.*, Nucl. Instrum. Methods Phys. Res. B **269**, 938 (2011).
[7] T. Hecht, H. Winter, A. G. Borisov, J. P. Gauyacq, and A. K. Kazansky, Phys. Rev. Lett. **84**, 2517 (2000).
[8] T. Hecht, H. Winter, A. G. Borisov, J. P. Gauyacq, and A. K. Kazansky, Faraday Discuss. **117**, 27 (2000).
[9] A. G. Borisov, A. Mertens, S. Wethekam, and H. Winter, Phys. Rev. A **68**, 012901 (2003).
[10] M. Alducin, V. M. Silkin, J. I. Juaristi, and E. V. Chulkov, Phys. Rev. A **67**, 032903 (2003).
[11] V. M. Silkin, J. M. Pitarke, E. V. Chulkov, and P. M. Echenique, Phys. Rev. B **72**, 115435 (2005).
[12] V. M. Silkin, M. Alducin, J. I. Juaristi, E. V. Chulkov, and P. M. Echenique, J. Phys. Condens. Matter **20**, 304209 (2007).
[13] N. Stolterfoht, J. H. Bremer, V. Hoffmann, R. Hellhammer, D. Fink, A. Petrov, and B. Sulik, Phys. Rev. Lett. **88**, 133201 (2002).
[14] L. Vattuone, M. Smerieri, T. Langer, C. Tegenkamp, H. Pfnur, V. M. Silkin, E. V. Chulkov, P. M. Echenique, and M. Rocca, Phys. Rev. Lett. **110**, 127405 (2013).
[15] B. Diaconescu *et al.*, Nature (London) **448**, 57 (2007).
[16] S. J. Park and R. E. Palmer, Phys. Rev. Lett. **105**, 016801 (2010).
[17] M. Jahn, M. Muller, M. Endlich, N. Neel, J. Kroger, V. Chis, and B. Hellsing, Phys. Rev. B **86**, 085453 (2012).
[18] K. Tőkési, X. M. Tong, C. Lemell, and J. Burgdörfer, Phys. Rev. A **72**, 022901 (2005).
[19] M. N. Faraggi, M. S. Gravielle, and V. M. Silkin, Phys. Rev. A **69**, 042901 (2004).
[20] C. D. Archubi, M. S. Gravielle, and V. M. Silkin, Phys. Rev. A **84**, 012901 (2011).
[21] E. V. Chulkov, V. M. Silkin, and P. M. Echenique, Surf. Sci. **391**, L1217 (1997); **437**, 330 (1999).
[22] M. N. Faraggi, M. S. Gravielle, M. Alducin, J. I. Juaristi, and V. M. Silkin, Phys. Rev. A **72**, 012901 (2005).
[23] C. A. Ríos Rubiano, M. S. Gravielle, D. M. Mitnik, and V. M. Silkin, Phys. Rev. A **85**, 043422 (2012).
[24] M. S. Gravielle, Phys. Rev. A **58**, 4622 (1998).
[25] A. G. Eguiluz, Phys. Rev. Lett. **51**, 1907 (1983).
[26] M. S. Gravielle and J. E. Miraglia, Phys. Rev. A **50**, 2425 (1994).
[27] J. F. Ziegler, J. P. Biersack, and U. Littmark, *The Stopping and Range of Ions in Solids* (Pergamon, New York, 1985), Vol. 1.
[28] R. A. Bartynski, R. H. Gaylord, T. Gustafsson, and E. W. Plummer, Phys. Rev. B **33**, 3644 (1986).
[29] R. Paniago, R. Matzdorf, G. Meister, and A. Goldmann, Surf. Sci. **336**, 113 (1995).
[30] E. V. Chulkov and V. M. Silkin, Solid State Commun. **58**, 273 (1986).
[31] E. V. Chulkov, V. M. Silkin, and E. N. Shirykalov, Surf. Sci. **188**, 287 (1987).
[32] E. E. Krasovskii and W. Schattke, Phys. Rev. B **59**, R15609 (1999).
[33] E. E. Krasovskii, V. N. Strocov, N. Barrett, H. Berger, W. Schattke, and R. Claessen, Phys. Rev. B **75**, 045432 (2007).
[34] M. S. Gravielle, Phys. Rev. A **62**, 062903 (2000).
[35] O. Grizzi, E. A. Sanchez, S. Lacombe, and V. A. Esaulov, Phys. Rev. B **68**, 085414 (2003).
[36] D. S. F. Crothers and J. F. McCann, J. Phys. B **16**, 3229 (1983).
[37] M. S. Gravielle and J. E. Miraglia, Phys. Rev. A **67**, 042901 (2003).
[38] J. E. Miraglia and M. S. Gravielle, Phys. Rev. A **81**, 042709 (2010).
[39] E. Clementi and C. Roetti, At. Data Nucl. Data Tables **14**, 177 (1974).
[40] K. Kimura, G. Andou, and K. Nakajima, Phys. Rev. Lett. **81**, 5438 (1998).
[41] C. C. Montanari, D. M. Mitnik, C. D. Archubi, and J. E. Miraglia, Phys. Rev. A **80**, 012901 (2009).
[42] The corresponding initial states were described by using Hartree-Fock wave functions for Mg^{++}, extracted from Ref. [39], p. 332.
[43] Notice that we are displaying $dP/d\vec{k}_f$, instead of $dP/dE_f d\Omega_f$, which shifts the energy position of the convoy peak.
[44] M. S. Gravielle, J. E. Miraglia, G. G. Otero, E. A. Sanchez, and O. Grizzi, Phys. Rev. A **69**, 042902 (2004).
[45] C. O. Reinhold and J. Burgdörfer, Phys. Rev. A **55**, 450 (1997).